TITLE:
Environmental and genetic disease modifiers of haploinsufficiency of A20

Running title:
Hominin TNFAIP3 variants influence Mendelian disease

Authors:
Nathan W. Zammit[1,3], Paul E. Gray[4,5,], Owen M. Siggs[1,6], Jin Yan Yap[1], Amanda Russell[1], Daniele Cultrone[1,3], Joanna Warren[1], Stacey N. Walters[1], Robert Brink[1,3], David Zahra[1,3], Deborah L. Burnett[1,3], Velimir Gayevskiy[2,3], Andre E. Minoche[2,3], John B. Ziegler[4,5], Maria E. Craig[5,7], Melanie Wong[8], Paul Benitez-Aguirre[9], Juliana Teo[10], Mark J. Cowley[4,11], Marcel E. Dinger[1,12], Stuart G. Tangye[1,3], Catherine Burke[13], Tri G. Phan[1,3], Christopher C. Goodnow[1,3], Shane T. Grey[1,3]

Affiliations:
[1]Immunity & Inflammation Theme, [2]Kinghorn Center for Clinical Genomics, Garvan Institute of Medical Research, Darlinghurst, NSW, 2010 Australia
[3]St Vincent's Clinical School, Faculty of Medicine, University of New South Wales Sydney, NSW 2145, Australia
[4]Department of Immunology and Infectious Diseases, Sydney Children's Hospital, Randwick NSW 2031, Australia
[5]School of Women's and Children's Health, University of New South Wales, Sydney, NSW 2010, Australia
[6]Department of Ophthalmology, Flinders University, Bedford Park, SA 5042 Australia
[7]Institute of Endocrinology and Diabetes, [8]Department of Allergy and Immunology, [9]Endocrinology Department, [10]Haematology Department, The Children's Hospital at Westmead, NSW 2045, Australia
[11]Children's Cancer Institute, Lowy Cancer Centre, UNSW Sydney, Kensington, NSW, Australia
[12]School of Biotechnology and Biomolecular Sciences, UNSW Sydney, NSW 2052, Australia
[13]School of Life Sciences, University of Technology Sydney, Sydney, NSW 2007, Australia

ABSTRACT

Monogenic diseases can often manifest diverse clinical phenotypes and cause diagnostic dilemmas. While monoallelic loss-of-function variants in *TNFAIP3* (Haploinsufficiency of A20; HA20) cause a highly penetrant autoinflammatory disease, the variable expressivity suggest a role for additional genetic and environmental disease modifiers. Here, we identify critically ill children who inherited a family-specific *TNFAIP3* deletion from one of their otherwise healthy parents. Each of the probands also inherited *in trans* a subtle loss-of-function I207L *TNFAIP3* variant that is common in Oceania, originally introgressed from Denisovans. Modelling this compound heterozgous state in mice under specific pathogen free conditions demonstrated a reduced threshold to break immune tolerance. Exaggerated immune responses were precipitated by inheriting the two genetic hits on the *TNFAIP3* checkpoint coupled with increasing the microbial challenge to immune tolerance, either by co-housing with pet store mice carrying a wild microbial burden or by transient dietary exposure to a chemical that diminishes the intestinal mucin barrier separating gut microbes from immune sensing systems. These data illuminate second-hit genetic and environmental modifiers contributing to complex inflammatory and autoimmune disease. Increased mechanistic understanding of the presence and contribution of disease modifiers will aid diagnostic and prognostic patient stratification and potentially reveal novel therapeutic opportunities.

INTRODUCTION

TNFAIP3 (tumor necrosis factor, alpha-induced protein 3) encodes A20, a highly conserved and evolutionarily ancient protein that serves as a key immune tolerance checkpoint by negatively regulating tissue inflammation and immune responses by inhibiting NF-κB signaling (1-4). A20 inhibits NF-κB signalling though catalytic and non-catalytic mechanisms. A20's ovarian tumor domain (OTU) and Zinc finger 4 region exert K63-deubiquitinating and K48-ubiqutinating activity, respectively, and co-operate to inactivate key signaling substrate proteins and target them for proteasomal degradation (5-8). In contrast, A20's Zinc finger 7 binds to linear ubiquitin chains disrupting IKK activation (9, 10). *TNFAIP3* transcription is induced by NF-κB (11-13) and A20's inhibitory activities are activated by IKKβ-mediated phosphorylation at Ser 381 (9, 14, 15), forming a negative feedback loop on NF-κB signaling.

Common variants at the *TNFAIP3* locus are associated with multiple polygenic autoimmune and inflammatory diseases (16), including type 1 diabetes, rheumatoid arthritis, systemic lupus erythematosus, psoriasis and Crohn's disease highlighting the importance of *TNFAIP3* in human health and disease. In contrast, haploinsufficiency of A20 (HA20) caused by *TNFAIP3* deletion or protein-truncating variants causes an autosomal dominant, childhood-onset inflammatory disease, reminiscent of Behcet's disease, with apparent complete penetrance (17). Subsequent findings have reported HA20 in patients with diverse autoimmune and inflammatory dysregulatory conditions including autoimmune lymphoproliferative syndrome (ALPS), systemic lupus erythematosus, type 1 diabetes, hepatitis and interstitial lung disease (18-24).

An emerging feature of HA20 is its association with diverse clinical presentations, phenotypes, and disease severity, even in individuals carrying the same variant, as well as a roughly two times higher incidence in females then men (19, 23-25). The recognition of diverse phenotypes, age of onset and gender bias, suggests a significant role for environmental and or genetic disease modifiers in patients with HA20. Such interactions have been described for

Mendelian diseases, including the identification of genes that can modify cystic fibrosis phenotypes in association with mutations in the *CFTR* gene (26), and both gene and environmental factors that influence Huntington's disease progression (27). However, few have been identified in the context of monogenic immune dysregulatory conditions.

Here, we identify critically ill children who inherited a *TNFAIP3* deletion from one of their otherwise healthy parents, challenging the hypothesis that A20 deficiency alone is always fully penetrant for disease. We now explain these apparently contradictory findings by providing evidence from mouse models for two additional disease modifiers contributing to HA20 in these patients. The first disease modifier is an inherited archaic *TNFAIP3* genetic variant that causes a subtle loss of A20 function, while the second disease modifier came in the form of an environmental challenge that altered microbiome composition. HA20 is a new disease and increased mechanistic understanding of the presence and contribution of disease modifiers will aid diagnostic and prognostic patient stratification and potentially reveal novel therapeutic opportunities.

RESULTS

Here, we studied two families, Family 1 of mixed Scottish-Fijian/Samoan ancestry and Family 2 of European and New Zealand Māori ancestry (Figure 1A), each with a child with early-onset inflammatory and autoimmune manifestations (Figure 1B, Supplementary Figure 1A,B). Both Child 1 (Family 1) and Child 2 (Family 2) presented with inflammatory bowel disease (IBD), autoantibodies, and cytopenia. Child 1 also exhibited ocular inflammation, subclinical thyroid disease and rhinitis, whereas Child 2 also presented with mouth and genital ulcers, arthralgia/arthritis and type 1 diabetes. Whole genome sequencing of the parent-proband trios revealed each family harbored a unique deletion at the *TNFAIP3* locus, present in both the proband and one unaffected parent respectively. The deletion in Family 1 spanned the entire *TNFAIP3* locus (g.137683250-139345585del; Figure 1C) and was confirmed by CGH array, while Family 2 harboured a 2bp frameshift deletion predicting a premature stop codon truncating the normal protein sequence (p.(N371Sfs*17)) (Figure 1D, Supplementary Figure 2). However, neither of the families had a history of childhood-onset inflammatory disease, despite the fact that an unaffected parent in each pedigree aged 59 and 40 respectively, carried the same heterozygous *TNFAIP3* loss of function allele as the affected proband (Figure 1A). Analysis of human sequence data from people without early onset disease (gnomAD v2.1.1) revealed only 2 from 141,456 individuals with heterozygous protein-truncating *TNFAIP3* mutations, compared to an expected rate of 32 individuals based on coding region size and composition (pLI=1, LOEUF=0.2) (28). Studies in vertebrate model organisms also reveal that HA20 does not always drive a disease phenotype, as mice and zebrafish heterozygous for *Tnfaip3* deletion present as healthy when housed under specific pathogen free (SPF) conditions (1, 3). This suggested that additional, but hitherto unknown, disease modifiers cooperate with *TNFAIP3* haploinsufficiency in these families to drive their disease phenotypes.

To explore the potential of additional genetic modifiers, we searched for *TNFAIP3* variants *in trans* with each deletion. In both probands we identified the same pair of missense variants *in*

122 *cis*, p.(T108A) and p.(I207L) (Figure 1D), which formed part of a larger haplotype consisting
123 of multiple coding and non-coding variants (15, 29). Both missense variants are within the
124 OTU domain of A20 (Figure 1E-G), and were rare within public variant databases (gnomAD
125 v2.1.1 allele frequency 0.0001169-0.0001202). We have previously shown, these variants are
126 enriched in populations in Oceania (15), representing 15-45% of all alleles in Polynesia (e.g.
127 Vanuatu), ~22% of alleles in Martu Australians, 31-48% of *TNFAIP3* alleles in people of the
128 eastern Indonesian islands (e.g. Flores), and 32-100% of alleles in Papuans. Analysis of the
129 genetic history of this haplotype revealed it was inherited by anatomically modern humans
130 from Denisovans ~50 kya (15, 29). The *TNFAIP3* Denisovan haplotype (hap) contains other
131 non-coding variants found not to impact *TNFAIP3* expression (15). In addition, I207 is
132 predicted to be the functional coding allele, as in contrast to T108, I207L is invariant across
133 most jawed vertebrates (Figure 1F) and has a higher *in-silico* deleterious score (CADD score
134 23.2; (15)). In transfected cells expressing *TNFAIP3* cDNA, the T108A;I207L substitutions
135 decreased A20 phosphorylation by IKKβ to 80% of wild-type, creating a subtle loss of NF-κB
136 inhibitory function (15). In both families, the T108A;I207L Denisovan haplotype was inherited
137 from one healthy parent and the *TNFAIP3* deletion from the other healthy parent (Figure 1A).
138 Hence, it was conceivable that co-inheritance of *TNFAIP3* haploinsufficiency and a subtle loss
139 of function Denisovan allele explained disease only in the child with both genetic hits in
140 compound heterozygous configuration.
141
142 To test if coinheritance of the two alleles had additive biochemical affects we performed
143 Western blot analysis of peripheral blood mononuclear cells (PBMCs) from healthy donors,
144 the heterozygous parents and the affected patients. A20 protein levels were decreased in
145 each of the deletion-carrying parents compared to healthy donors (Hd) (Figure 2A, B &
146 Supplementary Figure 3. A, C). Neither *TNFAIP3* deletion 1 (+/del1), spanning the entire
147 *TNFAIP3* locus, or deletion 2, a frameshift deletion p.(N371Sfs*17), encoded proteins that
148 could be detected by the antibody probe raised against the C-terminus region (aa 440-790) of
149 A20. Indeed, mRNA analysis of *TNFAIP3* levels using probes spanning exons 2 and 4 show

150 a dose dependent reduction for individuals in family 1 harboring a heterozygous deletion of
151 the entire *TNFAIP3* locus compared to 15 healthy donors (Figure 1C). Heterozygous carriers
152 of the I207L allele (+/hap) exhibited similar A20 protein levels to healthy donors, with probands
153 (hap/del) exhibiting levels similar to their +/del parent (Figure 2A, B & Supplementary Figure
154 3A, C). Active IKKβ also phosphorylates another NF-κB inhibitory protein, IκBα, which then
155 undergoes K48-linked ubiquitination and degradation to release active NF-κB (30, 31).
156 Western blot analysis revealed levels of IκBα were greatly decreased in PBMCs from the
157 del/hap probands in both families even under non-stimulated conditions (Figure 2A, B;
158 Supplementary Figure 3B, D). For family 1, PBMCs from the healthy parent with the *TNfAIP3*
159 deletion (+/del) exhibited more rapid loss of IκBα following TNF stimulation compared to
160 PBMCs from healthy donors (Figure 2A; Sup. Figure 3B), as previously reported for HA20
161 (17). However, this effect was less than the del/hap proband from this family (Figure 2A; Sup.
162 Figure 3B). In family 2, the healthy +/del parent exhibited greatly decreased IκBα similar to the
163 del/hap proband (Figure 2B; Sup. Figure 3D).
164
165 RT-PCR analysis of PBMCs was used to measure mRNA encoding NF-κB induced
166 inflammatory genes (30) before and following TNF stimulation. These target genes were more
167 strongly induced in cells from del/hap probands than in PBMCs from *TNFAIP3*$^{+/+}$ donors. Cells
168 from +/del individuals exhibited an intermediate phenotype, while +/hap cells showed a subtle
169 hyper-inflammatory response (Figure 2C, D). Collectively, these data are consistent with an
170 additive biochemical effect of coinheriting a *TNFAIP3* null/truncating and *TNFAIP3*
171 hypomorphic allele, but are not conclusive because of the small number of donors with the
172 relevant genotypes.
173
174 Given the limited availability of matched +/del and hap/del individuals to make conclusions
175 about additive effects, we generated two mouse lines by Cas9/CRISPR gene editing on the
176 genetically homogeneous C57BL/6 background, transmitting either a *Tnfaip3* truncating
177 mutation (p.Ala240Valfs*7, referred to as del) or a *Tnfaip3* T108A;I207L allele (hap) (15)

178 (Supplementary Figure 4A, B). Next we crossed both lines so that offspring would be wild-
179 type, heterozygous truncating (+/del), heterozygous T108A;I207L (+/hap), or compound
180 heterozygous (hap/del) to model the human family members (Figure 3A). *Tnfaip3* +/hap, +/del
181 and hap/del mice reared in SPF conditions exhibited normal weights at weaning and at 8
182 weeks of age (Figure 3B; Supplementary Figure 4C, D). Heterozygous loss of full length A20
183 due to the truncating allele was confirmed by a decrease to 50% of wild-type A20 protein levels
184 in isolated +/del and hap/del thymocytes (Figure 3C, D). Western blot analysis of TNF-
185 stimulated thymocytes revealed decreased IκBα protein levels even under non-stimulated
186 conditions for compound heterozygous hap/del cells that was not observed for thymocytes
187 from +/hap or +/del thymocytes (Figure 3C, E). *Tnfaip3* +/del cells exhibited a trend to
188 increased stimulus-dependent loss of IκBα compared to +/hap and WT cells (Figure 3C, E).
189 These findings highlight an additive role for +/del and +/hap *Tnfaip3* alleles in restraining NF-
190 κB inhibitory activity.
191
192 In contrast to the exaggerated biochemical response in the compound heterozygous mice,
193 flow cytometric analysis revealed comparable increases in the proportions of $CD44^{hi}CD62^{low}$
194 effector memory CD8 and CD4 T cell subsets in the spleen (Figure 3F) and mesenteric lymph
195 nodes (MLN, Figure 3G) of *Tnfaip3* +/del and hap/del mice compared to +/hap and wild-type
196 littermates (Supplementary Figure 5A-F). *Tnfaip3* +/del and hap/del mice also exhibited a
197 comparably increased proportion of FOXP3+ Tregs among CD4 T cells (Figure 3H, I), and
198 increased number of B cells in the spleen (Supplementary Figure 5G). However, only hap/del
199 mice exhibited significantly increased numbers of germinal center B cells in the spleen and
200 MLN under SPF conditions (Supplementary Figure 5I, J).
201
202 A major clinical phenotype in HA20 patients included gut pathology (Supplementary Figure
203 1A). Interestingly, mucosal inflammation is a unifying symptom of human HA20 disease (24,
204 32) and spontaneous gut inflammation observed in *Tnfaip3* gene-targeted mice is driven by
205 exaggerated responses to gut microbiota (33). Analysis of colon sections from SPF *Tnfaip3*

206 hap/del mice, revealed immune infiltrates with a mild clinical score similar to *Tnfaip3* +/del
207 mice, which was higher than that observed in *Tnfaip3* +/hap or wild-type littermates (Figure
208 3J, K).
209
210 The results above indicated that *Tnfaip3* haploinsufficiency (+/del) in mice causes subclinical
211 immune dysregulation that is not markedly increased by co-inheriting the hypomorphic I207L
212 allele when the microbial flora is highly controlled in an SPF facility. To better replicate natural
213 microbial stimulation of the immune system, we co-housed the *Tnfaip3* mutant mice with "dirty"
214 mice harboring a diverse microbiome. Cohousing mice with non-laboratory wild mice has been
215 shown to facilitate the horizontal transfer of microbiota, maturing the immune system (34, 35).
216 Deep sequencing of bacterial 16S rRNA of fecal pellets from the co-housed mice showed
217 horizontal transfer resulting in a more diverse gut microbiota compared to their SPF
218 counterparts, consisting of an increase in the relative abundance of Prevotella, Odoribacter,
219 Helicobacter, Muscispirillum and a decrease in Akkermansia. However, no discernible
220 difference in principle microbial components was observed among co-housed *Tnfaip3* hap/del,
221 +/del, +/hap and +/+ animals (Figure 4A; Supplementary Figure 6A, B). Cohousing did not
222 adversely affect the weight or survival of *Tnfaip3* wild-type, +/hap, +/del or hap/del mice
223 (Supplementary Figure 6C), but increased the percentage of $CD44^{hi}$ effector/memory CD4
224 and CD8 T cells in the blood within 1 week of cohousing (Supplementary Figure 6D, E).
225 Following 8 weeks of cohousing, clinical scores for colon inflammation tended to be higher in
226 *Tnfaip3* hap/del mice than +/del animals, with marked mononuclear infiltrates and goblet cell
227 hyperplasia (Figure 4B, C). In the MLN draining the gut, the proportion of effector/memory
228 cells among CD8 and CD4 T cells was increased in +/del mice and further increased in hap/del
229 compound heterozygotes (Figure 4D, E). A similar finding was observed when measuring total
230 CD44+ CD8 T cells (Supplementary Figure 5D), and CD4 central memory T cells in MLNs
231 (Supplementary Figure 5E, F). Cohousing with dirty mice did not segregate Treg frequencies
232 between *Tnfaip3* +/del and hap/del genotypes (Figure 4F, G) but significantly decreased mean
233 FOXP3 protein levels per cell in splenic Tregs of *Tnfaip3* hap/del mice compared to +/del mice

234 (Figure 4H). In cohoused mice, percentage of splenic germinal center B cells was
235 progressively increased according to *Tnfaip3* genotype consistent with additive effects of the
236 del and hap mutations (Supplementary Figure 5 H-J).
237
238 To test a different environmental stressor, we next challenged *Tnfaip3* hap/del mice
239 maintained in SPF conditions by adding 2.5% dextran sodium sulfate (DSS) to drinking water.
240 DSS thins the intestinal mucin barrier that normally promotes bacterial tolerance by physically
241 separating most gut microbiota from the intestinal epithelium. DSS was given for 5 days, then
242 removed (day 0) and weight loss and recovery monitored for 2 weeks. Weight loss was
243 exaggerated and recovery delayed in *Tnfaip3* +/del animals and these effects were worsened
244 in hap/del compound heterozygous animals (Figure 4I). Only *Tnfaip3* hap/del mice exhibited
245 significant weight loss over the test period compared to wild-type littermates. Two weeks post-
246 DSS removal, colons were collected and assessed for inflammatory cell infiltrate, erosion and
247 ulceration, hyperplasia and submucosa oedema and goblet cell and crypt loss. *Tnfaip3* hap/del
248 mice exhibited the highest clinical scores (Figure 4J, K). DSS challenge caused an increase
249 in effector/memory $CD44^{hi}$ CD8 T cells and $FOXP3^{+}$ Tregs for all genotypes assessed
250 (Supplementary Figure 7A-D). In Tregs, *Tnfaip3* hap/del mice treated with DSS exhibited a
251 significant decrease in mean FOXP3 protein per cell compared to wild-type littermates treated
252 with DSS, while +/del animals tended to be intermediate (Figure 4L, M). DSS treatment also
253 increased the frequency of neutrophils in the spleen and MLNs, with *Tnfaip3* hap/del mice
254 exhibiting higher frequency of splenic neutrophils compared to +/del alone and wild-type
255 littermates (Supplementary Figure 7E, F).

256 **DISCUSSION**

257 The findings here reveal how rare and common inherited variants in an important immune
258 tolerance checkpoint interact with environmental stressors to precipitate autoimmune and
259 inflammatory disease. Rare deletions in *TNFAIP3* have been considered to cause a fully
260 penetrant autosomal dominant, childhood-onset inflammatory/autoimmune disease by
261 haploinsufficiency (17). However, HA20 patients present with diverse clinical characteristics
262 and variable age of onset suggesting a role for additional disease modifiers. Here we describe
263 two children with clinical HA20 syndrome who inherited a family-specific, heterozygous
264 inactivating *TNFAIP3* deletion from one well parent and a subtle loss-of-function *TNFAIP3*
265 allele that is common in Oceania, from their other healthy parent (15, 29). Ex-vivo analysis of
266 patient cells demonstrates increased inflammation and NF-κB signaling in asymptomatic
267 deletion carriers, which is potentiated in symptomatic probands. This potentiation was
268 replicated in mice rendered compound heterozygous for a deletion and the common Oceanian
269 allele, precipitated by exposing the mice to diverse gut microbes or damaging the mucin barrier
270 between gut microbes and the body's microbe response systems. The families described here
271 demonstrate that contrary to current consensus (18-22), *TNFAIP3* haploinsuffucuency does
272 not always cause a fully-penetrant childhood-onset inflammatory disease, and that *TNFAIP3*-
273 associated inflammatory disease exemplifies interaction between environmental triggers and
274 common and rare inherited alleles.

275

276 Here we show for the first time that some people carrying a heterozygous TNFAIP3
277 deletion/truncating allele do not develop inflammatory/autoimmune disease. Why does this
278 occur? The animal experiments here support two explanations that are not mutually exclusive.
279 First, asymptomatic carriers may lack second genetic hits – single or multiple common
280 polymorphisms - that further compromise the *TNFAIP3* immune tolerance checkpoint. The
281 'gene dose' effect observed for *TNFAIP3* variants here may be analogous to the potentiation
282 of rare deletions in RBM8A by common *in trans* hypomorphic SNPs in the causation of the
283 thrombocytopenia with absent radii (TAR) syndrome (36). By contributing to compound

284 heterozygous inheritance of HA20, the Denisovan-derived I207L (*Tnfaip3* hap) is a rare
285 example of a variant with relevance both at a population and Mendelian level, analogous to
286 protection from severe Falciparum Malaria afforded by heterozygosity for sickle cell variants
287 (37).
288
289 Second, these genetically predisposed, asymptomatic individuals may not have had as much
290 pressure applied to the checkpoint by environmental microbes. These concepts build upon
291 Archibald Garrod's prototypic recessive "inborn error of metabolism", alkaptonuria (AKU) (38),
292 and the more common recessive disease phenylketonuria (PKU) (39), where the genetic dose
293 of mutations inactivating enzymes for phenylalanine and tyrosine metabolism cooperates with
294 the dietary load of these amino acids. Above a certain threshold, over time, accumulating
295 metabolic intermediates form toxic polymers on collagen (alkoptonuria) or unmetabolized
296 phenylalanine blocks transporters at the blood-brain barrier leading to developmental delay.
297 In the case of PKU, understanding the gene/environment cooperation enables disease
298 prevention by limiting dietary phenylalanine. For people with an underlying gene deficit in the
299 *TNFAIP3* immune tolerance checkpoint, it will be important to recognise these individuals early
300 and identify ways to minimise microbial stimuli that take them over a threshold into
301 inflammatory or autoimmune disease.
302
303 Exposing *Tnfaip3* hap/del mice to 'dirty mice' with 'wild' microbial flora or transiently introducing
304 DSS in the drinking water (40), revealed a significantly worse outcome for *Tnfaip3* hap/del
305 mice compared to single variant mice. A thick inner mucin layer secreted by intestinal goblet
306 cells normally serves a key role in tolerating microbial flora in the gut lumen. This is achieved
307 by physically separating them from bacterial-sensing receptors on and within intestinal
308 epithelial cells and lamina propria macrophages, notably Toll-like receptors (TLR) and NOD-
309 like receptors (NLR) that activate NF-κB. Oral DSS rapidly disrupts the mucin barrier to
310 increase bacterial contact with the epithelium (41, 42). The resulting stimulation of TLR- and
311 NLR-induced NF-κB activation will increase pressure on the *TNFAIP3* checkpoint to dampen

312 NF-κB signaling and maintain tolerance to the bacteria, providing an explanation for the
313 additive effects of compound heterozygous hap/del *TNFAIP3* mutations on DSS pathology.
314 Consistent with this interpretation, complete deletion of both TNFAIP3 alleles selectively in
315 murine intestinal epithelial cells cooperates with DSS treatment and gut flora to cause a similar
316 inflammatory bowel disease (43).
317
318 As opposed to dietary compromise to the mucin barrier, a number of the bacterial species that
319 were expanded in the intestine of the co-housed mice, have specialized mechanisms to
320 penetrate the mucin barrier and adhere directly to intestinal epithelium. Gram-negative
321 Prevotella species of the Bacteroidetes phylum and segmented filamentous bacteria
322 predispose to autoimmune disease (44, 45) by mechanisms that depend upon adherence to
323 intestinal epithelium (46, 47). Mucispirillum colonizes the mucin layer to provoke inflammatory
324 bowel disease in mice lacking NOD2 and CYBB NADPH oxidase (48). Helicobacter hepaticus
325 provokes colitis in IL-10 deficient mice (49). These expansions in bacterial species coincided
326 with a loss of Akkermansia that exhibit anti-inflammatory properties that maintain the mucin
327 barrier (50, 51). In mice with specific pathogen free flora, homozygous loss of TNFAIP3 in
328 intestinal epithelial cells and in intestinal macrophages results in a vicious cycle of microbe-
329 induced overproduction of TNF by macrophages and intestinal epithelial cell hyperproliferation
330 and apoptosis, depleting goblet cells and the mucin barrier (52). Collectively, these results
331 illustrate how genetics, diet and gut microbial flora cooperate to exceed tolerance thresholds.
332
333 A significant loss of FOXP3 MFI was observed in *Tnfaip3* hap/del Tregs following cohousing
334 and DSS treatment that was not observed for single variant mice, potentially explaining their
335 segregating phenotypes. Treg activation and expansion is NF-κB dependent via the TCR-
336 CARD11 pathway (53-55). This is further evidenced by expanded Treg populations observed
337 in the *Tnfaip3* variant mice (15). However, chronic inflammation and persistent NF-κB
338 activation can drive FOXP3 instability (56, 57) by preventing FOXP3 hypomethylation, which
339 requires CD28/NF-κB deprivation in developing Tregs (57). These data suggest that the

340 biallelic addition of +/hap and +/del, potentiates NF-κB activation under inflammatory
341 conditions, down-regulating FOXP3 expression. Indeed western blot analysis of TNF
342 stimulated thymocytes show an additive effect for *Tnfaip3* +/hap and +/del variants on the NF-
343 κB inhibitor, IκBα. As A20 haploinsufficiency lowers immune stimulatory thresholds, a loss of
344 FOXP3 expression would likely be detrimental contributing to clinical inflammatory conditions
345 (58-61).
346
347 The experimental approaches deployed here possess real potential in the study of both HA20
348 and polygenic inflammatory bowel disease (IBD). The failure of mouse avatars representing
349 the genetics of human monogenic inflammatory disease to express a clinical phenotype unless
350 specifically challenged is not unique, with *Lrba* gene-deficient animals requiring DSS
351 stimulation to develop clinical disease (62). The models of colitis presented here associated
352 with mice having a more 'wild-type' intestinal flora contributes to growing knowledge for human
353 IBD where the search for pathogenic mechanisms is increasingly focused on changes to the
354 intestinal microbiota (63).
355
356 In summary, we demonstrate for the first time, incomplete penetrance associated with
357 deletions in *TNFAIP3*. The Oceanic allele that contains the functional p.I207L allele represents
358 a unique example of a common variant contributing to a Mendelian inflammatory disease, and
359 has implications for genomic filtering strategies, which might remove such variants.
360 Furthermore, *TNFAIP3* T108A;I207L which was adaptively introgressed into Oceanian
361 populations and can potentially provide resistance to infection (15), may represent the first
362 example of an immune variant with a population protective benefit, that is Mendelian
363 deleterious. It remains to be seen whether this same variant influences immunity and
364 inflammation in other non-Mendelian diseases in the large number of individuals who carry it
365 today. Finally, our data highlight the significance of ancestry in rare disease penetrance, and
366 the value of studying inherited disease in non-European populations, which are poorly
367 represented in current clinical and population genetic studies.

368 **REFERENCES**
369
370 1. Lee EG, Boone DL, Chai S, Libby SL, et al. Failure to regulate TNF-induced NF-kappaB and cell
371 death responses in A20-deficient mice. Science. 2000;289(5488):2350-4.
372 2. Boone DL, Turer EE, Lee EG, Ahmad RC, et al. The ubiquitin-modifying enzyme A20 is
373 required for termination of Toll-like receptor responses. Nat Immunol. 2004;5(10):1052-60.
374 3. Cultrone D, Zammit NW, Self E, Postert B, et al. A zebrafish functional genomics model to
375 investigate the role of human A20 variants in vivo. Scientific reports. 2020;10(1):19085.
376 4. Zammit NW, Walters SN, Seeberger KL, O'Connell PJ, et al. A20 as an immune tolerance
377 factor can determine islet transplant outcomes. JCI Insight. 2019;4(21).
378 5. Wertz IE, O'Rourke KM, Zhou H, Eby M, et al. De-ubiquitination and ubiquitin ligase domains
379 of A20 downregulate NF-kappaB signalling. Nature. 2004;430(7000):694-9.
380 6. Evans PC, Ovaa H, Hamon M, Kilshaw PJ, et al. Zinc-finger protein A20, a regulator of
381 inflammation and cell survival, has de-ubiquitinating activity. Biochem J. 2004;378(Pt 3):727-34.
382 7. Lu TT, Onizawa M, Hammer GE, Turer EE, et al. Dimerization and ubiquitin mediated
383 recruitment of a20, a complex deubiquitinating enzyme. Immunity. 2013;38(5):896-905.
384 8. Bosanac I, Wertz IE, Pan B, Yu C, et al. Ubiquitin binding to A20 ZnF4 is required for
385 modulation of NF-kappaB signaling. Mol Cell. 2010;40(4):548-57.
386 9. Wertz IE, Newton K, Seshasayee D, Kusam S, et al. Phosphorylation and linear ubiquitin
387 direct A20 inhibition of inflammation. Nature. 2015;528(7582):370-5.
388 10. Verhelst K, Carpentier I, Kreike M, Meloni L, et al. A20 inhibits LUBAC-mediated NF-kappaB
389 activation by binding linear polyubiquitin chains via its zinc finger 7. EMBO J. 2012;31(19):3845-55.
390 11. Liuwantara D, Elliot M, Smith MW, Yam AO, et al. Nuclear factor-kappaB regulates beta-cell
391 death: a critical role for A20 in beta-cell protection. Diabetes. 2006;55(9):2491-501.
392 12. Dixit VM, Green S, Sarma V, Holzman LB, et al. Tumor necrosis factor-alpha induction of
393 novel gene products in human endothelial cells including a macrophage-specific chemotaxin. Journal
394 of Biological Chemistry. 1990;265(5):2973-8.
395 13. Krikos A, Laherty CD, Dixit VM. Transcriptional activation of the tumor necrosis factor alpha-
396 inducible zinc finger protein, A20, is mediated by kappa B elements. J Biol Chem. 1992;267:17971-6.
397 14. Hutti JE, Turk BE, Asara JM, Ma A, et al. IkappaB kinase beta phosphorylates the K63
398 deubiquitinase A20 to cause feedback inhibition of the NF-kappaB pathway. Mol Cell Biol.
399 2007;27(21):7451-61.
400 15. Zammit NW, Siggs OM, Gray PE, Horikawa K, et al. Denisovan, modern human and mouse
401 TNFAIP3 alleles tune A20 phosphorylation and immunity. Nat Immunol. 2019;20(10):1299-310.
402 16. Ma A, Malynn BA. A20: linking a complex regulator of ubiquitylation to immunity and human
403 disease. Nat Rev Immunol. 2012;12(11):774-85.
404 17. Zhou Q, Wang H, Schwartz DM, Stoffels M, et al. Loss-of-function mutations in TNFAIP3
405 leading to A20 haploinsufficiency cause an early-onset autoinflammatory disease. Nat Genet.
406 2016;48(1):67-73.
407 18. Duncan CJA, Dinnigan E, Theobald R, Grainger A, et al. Early-onset autoimmune disease due
408 to a heterozygous loss-of-function mutation in TNFAIP3 (A20). Ann Rheum Dis. 2017.
409 19. Kadowaki T, Ohnishi H, Kawamoto N, Hori T, et al. Haploinsufficiency of A20 causes
410 autoinflammatory and autoimmune disorders. J Allergy Clin Immunol. 2017.
411 20. Ohnishi H, Kawamoto N, Seishima M, Ohara O, et al. A Japanese family case with juvenile
412 onset Behcet's disease caused by TNFAIP3 mutation. Allergol Int. 2017;66(1):146-8.
413 21. Shigemura T, Kaneko N, Kobayashi N, Kobayashi K, et al. Novel heterozygous C243Y
414 A20/TNFAIP3 gene mutation is responsible for chronic inflammation in autosomal-dominant
415 Behcet's disease. RMD Open. 2016;2(1):e000223.
416 22. Takagi M, Ogata S, Ueno H, Yoshida K, et al. Haploinsufficiency of TNFAIP3 (A20) by germline
417 mutation is involved in autoimmune lymphoproliferative syndrome. J Allergy Clin Immunol.
418 2017;139(6):1914-22.

419 23. Aeschlimann FA, Batu ED, Canna SW, Go E, et al. A20 haploinsufficiency (HA20): clinical
420 phenotypes and disease course of patients with a newly recognised NF-kB-mediated
421 autoinflammatory disease. Ann Rheum Dis. 2018;77(5):728-35.
422 24. Berteau F, Rouviere B, Nau A, Le Berre R, et al. 'A20 haploinsufficiency (HA20): clinical
423 phenotypes and disease course of patients with a newly recognised NF-kB-mediated
424 autoinflammatory disease'. Ann Rheum Dis. 2019;78(5):e35.
425 25. He T, Huang Y, Luo Y, Xia Y, et al. Haploinsufficiency of A20 Due to Novel Mutations in
426 TNFAIP3. J Clin Immunol. 2020;40(5):741-51.
427 26. Guggino WB, Stanton BA. New insights into cystic fibrosis: molecular switches that regulate
428 CFTR. Nature reviews Molecular cell biology. 2006;7(6):426-36.
429 27. Wexler NS, Lorimer J, Porter J, Gomez F, et al. Venezuelan kindreds reveal that genetic and
430 environmental factors modulate Huntington's disease age of onset. Proc Natl Acad Sci U S A.
431 2004;101(10):3498-503.
432 28. Karczewski KJ, Francioli LC, Tiao G, Cummings BB, et al. The mutational constraint spectrum
433 quantified from variation in 141,456 humans. Nature. 2020;581(7809):434-43.
434 29. Gittelman RM, Schraiber JG, Vernot B, Mikacenic C, et al. Archaic Hominin Admixture
435 Facilitated Adaptation to Out-of-Africa Environments. Curr Biol. 2016;26(24):3375-82.
436 30. Karin M, Ben-Neriah Y. Phosphorylation meets ubiquitination: the control of NF-[kappa]B
437 activity. Annu Rev Immunol. 2000;18:621-63.
438 31. Mathes E, O'Dea EL, Hoffmann A, Ghosh G. NF-kappaB dictates the degradation pathway of
439 IkappaBalpha. EMBO J. 2008;27(9):1357-67.
440 32. Aeschlimann FA, Laxer RM. Haploinsufficiency of A20 and other paediatric inflammatory
441 disorders with mucosal involvement. Curr Opin Rheumatol. 2018;30(5):506-13.
442 33. Turer EE, Tavares RM, Mortier E, Hitotsumatsu O, et al. Homeostatic MyD88-dependent
443 signals cause lethal inflammation in the absence of A20. J Exp Med. 2008;205(2):451-64.
444 34. Beura LK, Hamilton SE, Bi K, Schenkel JM, et al. Normalizing the environment recapitulates
445 adult human immune traits in laboratory mice. Nature. 2016;532(7600):512-6.
446 35. Rosshart SP, Herz J, Vassallo BG, Hunter A, et al. Laboratory mice born to wild mice have
447 natural microbiota and model human immune responses. Science. 2019;365(6452).
448 36. Albers CA, Paul DS, Schulze H, Freson K, et al. Compound inheritance of a low-frequency
449 regulatory SNP and a rare null mutation in exon-junction complex subunit RBM8A causes TAR
450 syndrome. Nat Genet. 2012;44(4):435-9, S1-2.
451 37. Hebbel RP. Sickle hemoglobin instability: a mechanism for malarial protection. Redox Rep.
452 2003;8(5):238-40.
453 38. Phornphutkul C, Introne WJ, Perry MB, Bernardini I, et al. Natural history of alkaptonuria. N
454 Engl J Med. 2002;347(26):2111-21.
455 39. Blau N, van Spronsen FJ, Levy HL. Phenylketonuria. Lancet. 2010;376(9750):1417-27.
456 40. Hakansson A, Tormo-Badia N, Baridi A, Xu J, et al. Immunological alteration and changes of
457 gut microbiota after dextran sulfate sodium (DSS) administration in mice. Clin Exp Med.
458 2015;15(1):107-20.
459 41. Johansson ME, Gustafsson JK, Sjoberg KE, Petersson J, et al. Bacteria penetrate the inner
460 mucus layer before inflammation in the dextran sulfate colitis model. PLoS One. 2010;5(8):e12238.
461 42. Johansson ME, Gustafsson JK, Holmen-Larsson J, Jabbar KS, et al. Bacteria penetrate the
462 normally impenetrable inner colon mucus layer in both murine colitis models and patients with
463 ulcerative colitis. Gut. 2014;63(2):281-91.
464 43. Vereecke L, Sze M, Mc Guire C, Rogiers B, et al. Enterocyte-specific A20 deficiency sensitizes
465 to tumor necrosis factor-induced toxicity and experimental colitis. J Exp Med. 2010;207(7):1513-23.
466 44. Scher JU, Sczesnak A, Longman RS, Segata N, et al. Expansion of intestinal Prevotella copri
467 correlates with enhanced susceptibility to arthritis. Elife. 2013;2:e01202.
468 45. Iljazovic A, Roy U, Galvez EJC, Lesker TR, et al. Perturbation of the gut microbiome by
469 Prevotella spp. enhances host susceptibility to mucosal inflammation. Mucosal Immunol. 2020.

470 46. Atarashi K, Tanoue T, Ando M, Kamada N, et al. Th17 Cell Induction by Adhesion of Microbes
471 to Intestinal Epithelial Cells. Cell. 2015;163(2):367-80.
472 47. Larsen JM. The immune response to Prevotella bacteria in chronic inflammatory disease.
473 Immunology. 2017;151(4):363-74.
474 48. Caruso R, Mathes T, Martens EC, Kamada N, et al. A specific gene-microbe interaction drives
475 the development of Crohn's disease-like colitis in mice. Sci Immunol. 2019;4(34).
476 49. Kullberg MC, Ward JM, Gorelick PL, Caspar P, et al. Helicobacter hepaticus triggers colitis in
477 specific-pathogen-free interleukin-10 (IL-10)-deficient mice through an IL-12- and gamma interferon-
478 dependent mechanism. Infect Immun. 1998;66(11):5157-66.
479 50. Gobert AP, Sagrestani G, Delmas E, Wilson KT, et al. The human intestinal microbiota of
480 constipated-predominant irritable bowel syndrome patients exhibits anti-inflammatory properties.
481 Scientific reports. 2016;6:39399.
482 51. Zhai R, Xue X, Zhang L, Yang X, et al. Strain-Specific Anti-inflammatory Properties of Two
483 Akkermansia muciniphila Strains on Chronic Colitis in Mice. Front Cell Infect Microbiol. 2019;9:239.
484 52. Vereecke L, Vieira-Silva S, Billiet T, van Es JH, et al. A20 controls intestinal homeostasis
485 through cell-specific activities. Nature communications. 2014;5:5103.
486 53. Altin JA, Tian L, Liston A, Bertram EM, et al. Decreased T-cell receptor signaling through
487 CARD11 differentially compromises forkhead box protein 3-positive regulatory versus T(H)2 effector
488 cells to cause allergy. J Allergy Clin Immunol. 2011;127(5):1277-85 e5.
489 54. Ronin E, Lubrano di Ricco M, Vallion R, Divoux J, et al. The NF-kappaB RelA Transcription
490 Factor Is Critical for Regulatory T Cell Activation and Stability. Frontiers in immunology.
491 2019;10:2487.
492 55. Oh H, Grinberg-Bleyer Y, Liao W, Maloney D, et al. An NF-kappaB Transcription-Factor-
493 Dependent Lineage-Specific Transcriptional Program Promotes Regulatory T Cell Identity and
494 Function. Immunity. 2017;47(3):450-65 e5.
495 56. Zhang Z, Zhang W, Guo J, Gu Q, et al. Activation and Functional Specialization of Regulatory T
496 Cells Lead to the Generation of Foxp3 Instability. J Immunol. 2017;198(7):2612-25.
497 57. Mikami N, Kawakami R, Chen KY, Sugimoto A, et al. Epigenetic conversion of conventional T
498 cells into regulatory T cells by CD28 signal deprivation. Proc Natl Acad Sci U S A. 2020;117(22):12258-
499 68.
500 58. Salama AD, Chitnis T, Imitola J, Ansari MJ, et al. Critical role of the programmed death-1 (PD-
501 1) pathway in regulation of experimental autoimmune encephalomyelitis. J Exp Med.
502 2003;198(1):71-8.
503 59. Free ME, Bunch DO, McGregor JA, Jones BE, et al. Patients with antineutrophil cytoplasmic
504 antibody-associated vasculitis have defective Treg cell function exacerbated by the presence of a
505 suppression-resistant effector cell population. Arthritis Rheum. 2013;65(7):1922-33.
506 60. Valencia X, Yarboro C, Illei G, Lipsky PE. Deficient CD4+CD25high T regulatory cell function in
507 patients with active systemic lupus erythematosus. J Immunol. 2007;178(4):2579-88.
508 61. Ooi JD, Snelgrove SL, Engel DR, Hochheiser K, et al. Endogenous foxp3(+) T-regulatory cells
509 suppress anti-glomerular basement membrane nephritis. Kidney Int. 2011;79(9):977-86.
510 62. Wang KW, Zhan X, McAlpine W, Zhang Z, et al. Enhanced susceptibility to chemically induced
511 colitis caused by excessive endosomal TLR signaling in LRBA-deficient mice. Proc Natl Acad Sci U S A.
512 2019;116(23):11380-9.
513 63. Chen H, Li H, Liu Z. Interplay of intestinal microbiota and mucosal immunity in inflammatory
514 bowel disease: a relationship of frenemies. Therap Adv Gastroenterol. 2020;13:1756284820935188.
515 64. Mevissen TE, Kulathu Y, Mulder MP, Geurink PP, et al. Molecular basis of Lys11-polyubiquitin
516 specificity in the deubiquitinase Cezanne. Nature. 2016;538(7625):402-5.
517 65. Siggs OM, Russell A, Singh-Grewal D, Wong M, et al. Preponderance of CTLA4 Variation
518 Associated With Autosomal Dominant Immune Dysregulation in the MYPPPY Motif. Frontiers in
519 immunology. 2019;10:1544.

520 66. Gayevskiy V, Roscioli T, Dinger ME, Cowley MJ. Seave: a comprehensive web platform for
521 storing and interrogating human genomic variation. bioRxiv. 2018.
522 67. Minoche AE, Lundie B, Peters GB, Ohnesorg T, et al. ClinSV: Clinical grade structural and copy
523 number variant detection from whole genome sequencing data. medRxiv.
524 2020(2020.06.30.20143453).
525 68. Bolyen E, Rideout JR, Dillon MR, Bokulich NA, et al. Reproducible, interactive, scalable and
526 extensible microbiome data science using QIIME 2. Nature biotechnology. 2019;37(8):852-7.
527 69. Martin M. Cutadapt removes adapter sequences from high-throughput sequencing reads.
528 EMBnetjournal. 2011;17(1):10-2.
529 70. Rognes T, Flouri T, Nichols B, Quince C, et al. VSEARCH: a versatile open source tool for
530 metagenomics. PeerJ. 2016;4:e2584.
531 71. Amir A, McDonald D, Navas-Molina JA, Kopylova E, et al. Deblur Rapidly Resolves Single-
532 Nucleotide Community Sequence Patterns. mSystems. 2017;2(2).
533 72. Bokulich NA, Kaehler BD, Rideout JR, Dillon M, et al. Optimizing taxonomic classification of
534 marker-gene amplicon sequences with QIIME 2's q2-feature-classifier plugin. Microbiome.
535 2018;6(1):90.
536 73. Mandal S, Van Treuren W, White RA, Eggesbo M, et al. Analysis of composition of
537 microbiomes: a novel method for studying microbial composition. Microb Ecol Health Dis.
538 2015;26:27663.
539 74. McMurdie PJ, Holmes S. phyloseq: an R package for reproducible interactive analysis and
540 graphics of microbiome census data. PLoS One. 2013;8(4):e61217.
541 75. Hamady M, Lozupone C, Knight R. Fast UniFrac: facilitating high-throughput phylogenetic
542 analyses of microbial communities including analysis of pyrosequencing and PhyloChip data. ISME J.
543 2010;4(1):17-27.
544 76. M.J. A. Permutational multivariate analysis of variance (PERMANOVA). In: N. Balakrishnan
545 TC, B. Everitt, W. Piegorsch, F. Ruggeri and J.L. Teugels, editor. Wiley StatsRef: Statistics References
546 Online2017.
547 77. Oksanen JF, Blanchet G, Friendly M, Kindt R, et al. Vegan: Community Ecology Package. R
548 package version 2.5-6. https://CRAN.R-project.org/package=vegan2019 [
549 78. Faith DP. Conservation evaluation and phylogenetic diversity. Biological Conservation.
550 1992;61(1):1-10.
551 79. Kembel SW, Cowan PD, Helmus MR, Cornwell WK, et al. Picante: R tools for integrating
552 phylogenies and ecology. Bioinformatics. 2010;26(11):1463-4.
553 80. Wickham H., François R, Henry L, Müller K. dplyr: A Grammar of Data Manipulation. R
554 package version 1.0.2. https://CRAN.R-project.org/package=dplyr2020 [
555 81. Erben U, Loddenkemper C, Doerfel K, Spieckermann S, et al. A guide to histomorphological
556 evaluation of intestinal inflammation in mouse models. Int J Clin Exp Pathol. 2014;7(8):4557-76.
557 82. Untergasser A, Cutcutache I, Koressaar T, Ye J, et al. Primer3--new capabilities and
558 interfaces. Nucleic Acids Res. 2012;40(15):e115.
559 83. Meyer M, Kircher M, Gansauge MT, Li H, et al. A high-coverage genome sequence from an
560 archaic Denisovan individual. Science. 2012;338(6104):222-6.

561

FUNDING:

N.W.Z was supported by an Australian Postgraduate Award and is an International Pancreas and Islet Transplant Association (IPITA) Derek Gray Fellow. The Clinical Immunogenomics Research Consortium of Australasia (CIRCA) was supported by the Jeffrey Modell Foundation, the John Brown Cook Foundation, and the Sydney Children's Hospital Network. N.W.Z was supported by an Australian Postgraduate Award and is supported by the International Pancreas and Islet Transplant Association (IPITA) Derek Gray Scholarship. S.G.T was a Principal Research Fellow (1042925) and is currently an Investigator (Leadership 3) of the NHMRC. C.C.G. was supported by the Bill and Patricia Ritchie Chair and by an NHMRC Senior Principal Research Fellowship. The research was supported by grants to C.C.G. from the NIH (AI52127, AI054523, AI100627) and NHMRC (1016953, 585490, 1081858), D.L.B from the NHMRC (1176351) and to S.T.G. from the NIH (DK076169) and NHMRC (1130222, 1140691). S.T.G. was supported by an NHMRC Senior Research Fellowship (1140691).

AUTHOR CONTRIBUTIONS:

CCG – project initiation, coordination, and data interpretation.

PEG, OMS, AR, JBZ, MEC, PB-A, JT, MW, MJC, VG, AEM, MED, CCG – Clinical recruitment, whole genome sequencing analysis of HA20 patients.

NWZ, JYY, SGT, AR, STG – Molecular and immune phenotyping of human PBMCs.

NWZ, DC, STG – molecular characterization of A20 variants.

NWZ, JW, SNW, DC, RB, DZ, DLB, STG – mouse avatar characterization, pathology and disease models.
NWZ, CB, TP, STG – Microbiome challenge (DSS model; cohousing model) and microbiome analysis.

NWZ, PEG, OMS, CCG, STG - analysed data and co-wrote the manuscript.

ACKNOWLEDGMENTS:

We thank the Biological Testing Facility at the Garvan Institute of Medical Research for animal care.

We thank the Clinical Immunogenomics Research Consortium of Australasia for collecting and co-ordinating human samples (CIRCA).
https://www.garvan.org.au/research/collaborative-programs/circa/about-circa.

COMPETING INTERESTS:

All authors declare they have no competing interests as defined by Nature Research, or other interests that might be perceived to influence the results and/or discussion reported in this paper.

DATA AVAILABILITY:

The data that support the findings of this study are available from the corresponding author upon request

FIGURES AND FIGURE LEGENDS:

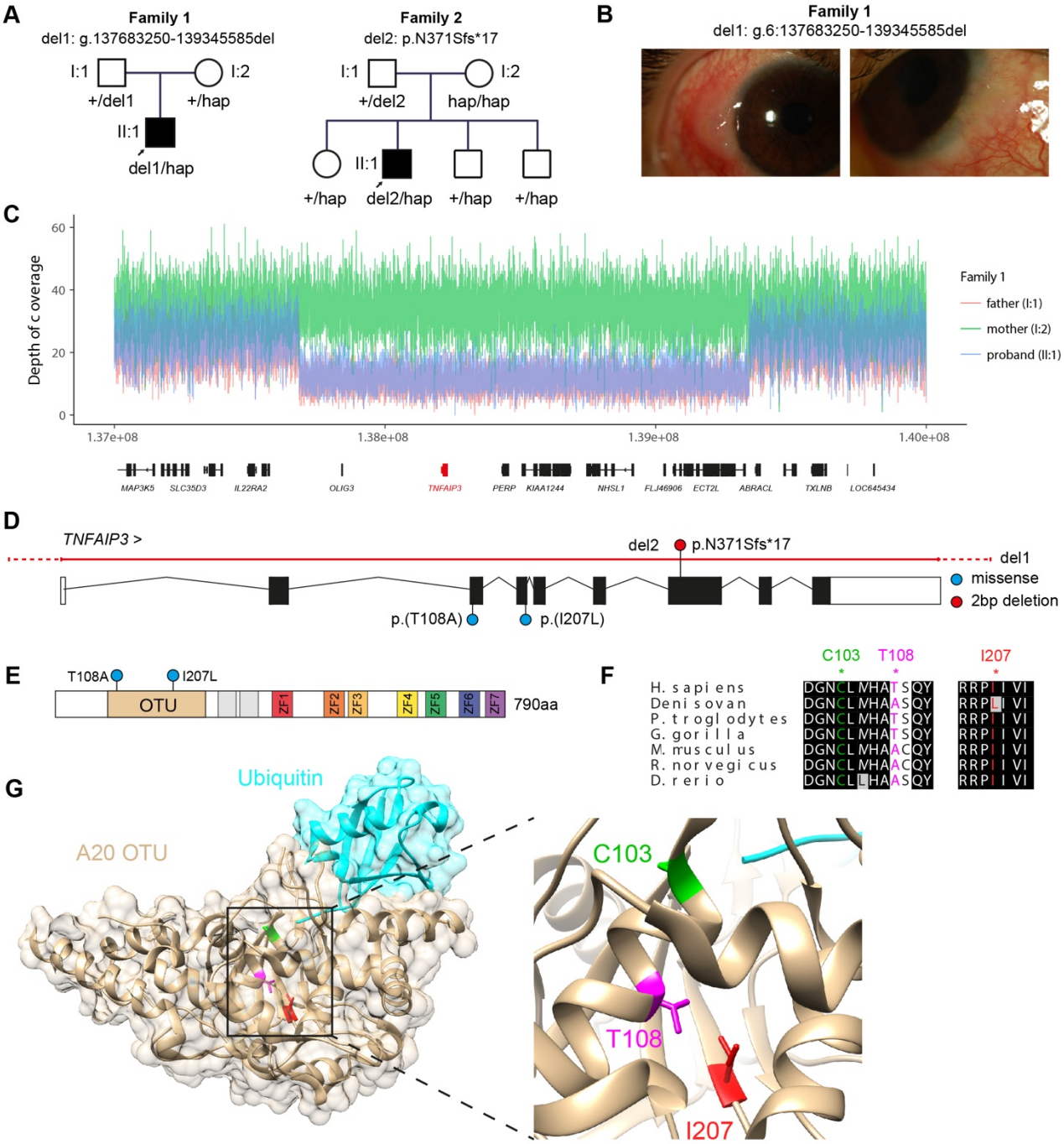

Figure 1: HA20 probands harbour a coding denisovan introgressed *TNFAIP3* allele in *trans* to A20 deletion.

(A) Family trio's of identified probands. (**B)** Photo of ocular inflammation from proband of family 1. (**C)** Sequencing coverage map depicting deletion of locus spanning *TNFAIP3. (***D)** Schematic demonstrating the location of HA20 variants del1 from family 1 and del2 from family 2. Each HA20 deletion is located *in trans* to two *in cis* missense variants T108A and I207L, located in exons 3 and 4 of *TNFAIP3,* respectively. T108A and I207L formed part of a larger haplotype adaptively introgressed from Denisovan Hominins (15, 29), referred to as hap in A. (**E)** Location of *TNFAIP3* hap missense variants, T108A and I207L in reference to the primary protein structure of A20. OTU = ovarian tumor

617 domain. ZF = Zinc finger. **(F)** Conservation and (**G)** location of T108 and I207 alleles in context with the
618 OTU domain catalytic 103 (5LRX)(64).

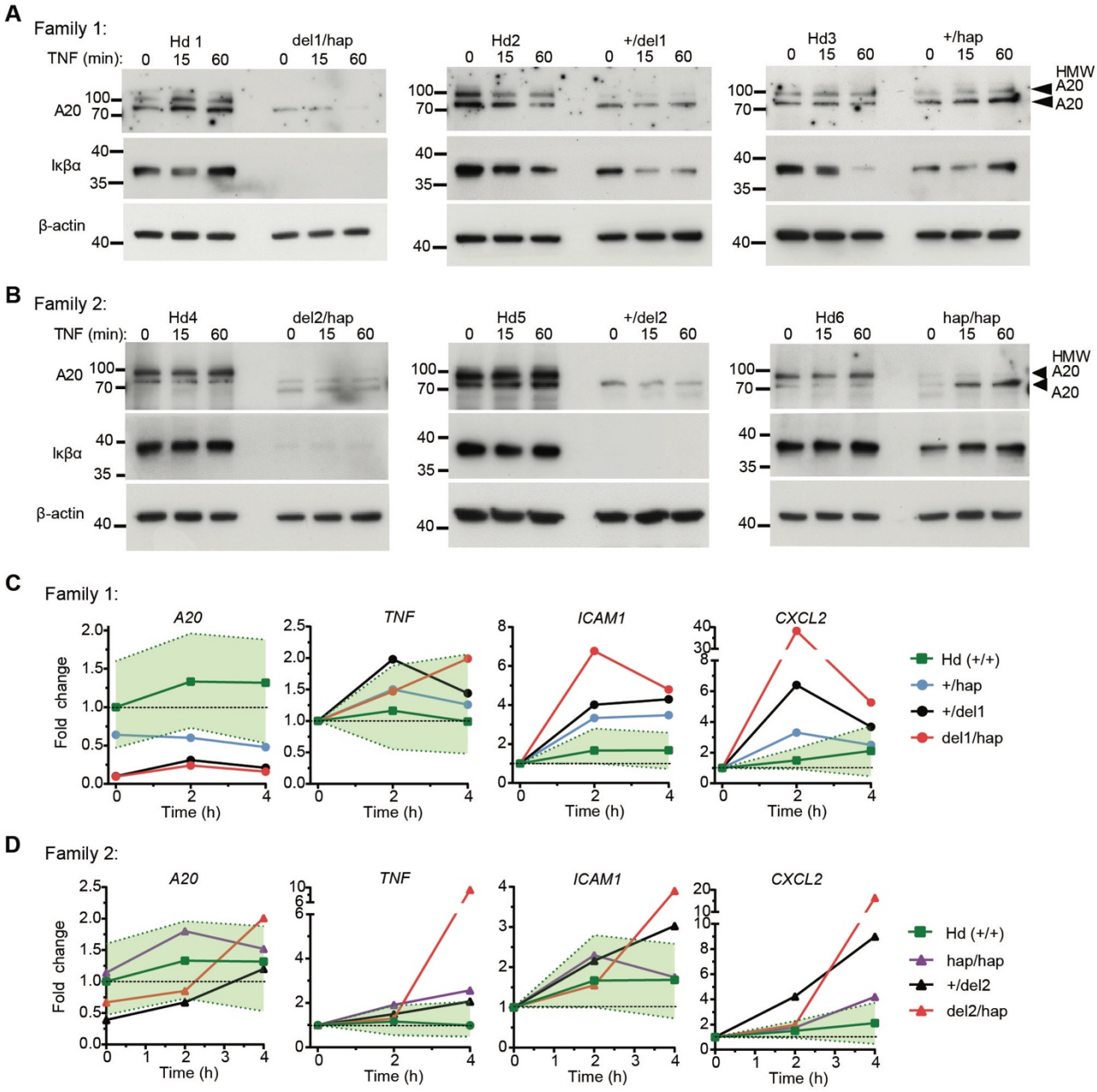

Figure 2: **Analysis of peripheral blood mononuclear cells (PBMCs) from parent-proband Trios.** **(A-B)** Immunoblot analysis of PBMCs from parent-proband trios from family 1 **(A)** and family 2 **(B)**. Probands from each family harbor a *TNFAIP3* deletion (del1 or 2) and the *TNFAIP3* T108A;I207L oceanic haplotype (hap) in *trans* (del/hap). Parents are either heterozygous for a *TNFAIP3* del or heterozygous or homozygous for the *TNFAIP3* hap allele. PBMCs were left untreated or stimulated with TNF for 15 or 60 min. Proteins assessed included A20, IκBα and β-actin (loading control). A20 high-molecular weight bands (HMW) representing phospho-A20 are indicated (9, 14, 15). Healthy donors = Hd. Immunoblots of PBMC lysates from +/Hap and hap/hap parents (right panels) have been previously reported (15)(ref). **(C-D)**, RT–PCR analysis of *TNFAIP3*, *TNF, ICAM1* and *CXCL2* gene expression in PBMCs from proband trios in A and B. Probands (red), +/hap (blue), hap/hap (purple), +/del (black) and 15 healthy donors (green) +/- range (shaded light green).

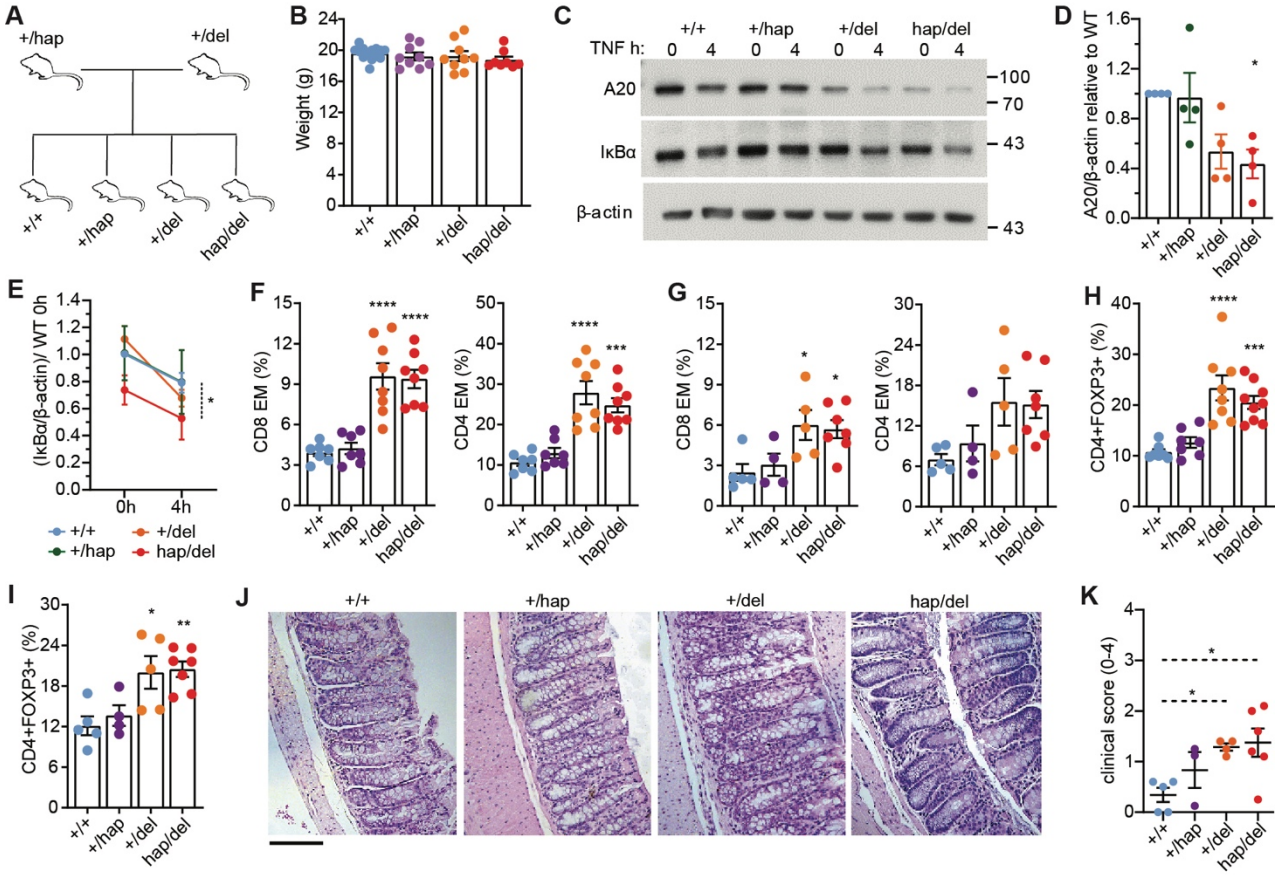

Figure 3: Molecular and phenotypical analysis of hap/del mice.

(A) Pedigree tree illustrating breeding strategy for *Tnfaip3* hap/del line. **(B)** Weight of 8-week-old female *Tnfaip3* hap/del mice of the indicated genotype. **(C)** Representative immunoblot of thymocyte lysates isolated from mice with indicated genotypes and stimulated with TNF for indicated times. Proteins probed include A20, IκBα and loading control β-actin. Cumulative densitometry is shown for **(D)** A20 and **(E)** IκBα with each point representing thymocytes from an individual mouse. **(F-G)** Percentage CD44hiCD62Lo effector memory cells among CD8+ or CD4+ T cells from the spleen (F) or Mesenteric lymph node (G) of mice with the indicated genotype. **(H-I)** Percentage of FOXP3+ regulatory T cells among CD4+ cells from the spleens (H) or mesenteric lymph nodes **(I)** of mice of the indicated genotypes. Flow cytometric data are cumulative from 3 independent experiments. **(J)** Representative sections showing H&E-stained colons from female mice of the indicated genotype. Scale bar = 200 µm. **(K)** Clinical score of representative colons shown in (J). Statistical analysis was performed by one-way anova ANOVA with Tukey post hoc test, and data shown as the mean +/- s.e.m: *P<0.05; ***P* < 0.01; ****P* < 0.001; *****P* < 0.0001.

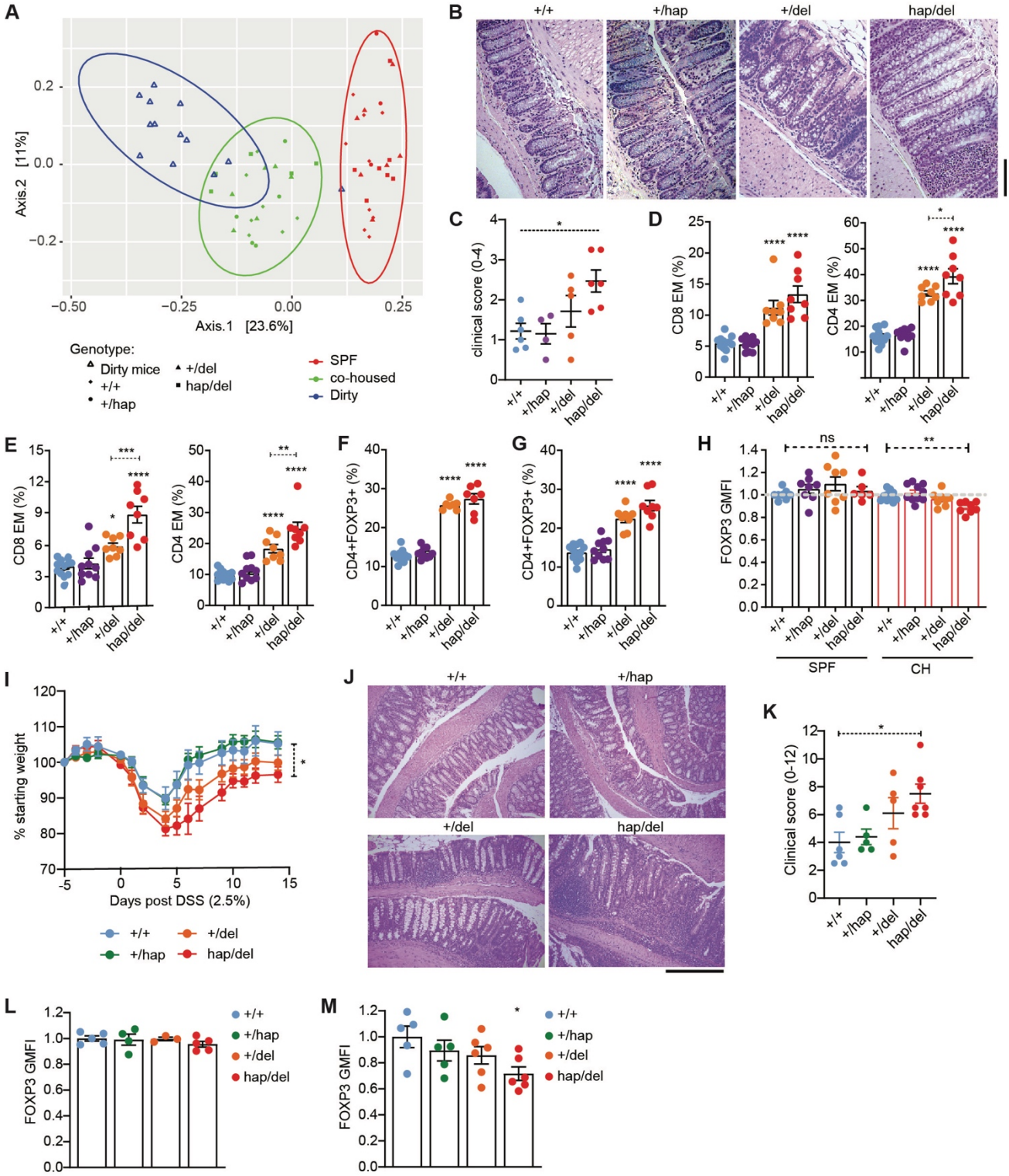

Figure 4: Microbiome and DSS challenge uncovers differential effects for hap/del mice compared to +/del alone.

(A) Unweighted unifrac PCoA showing cohoused *Tnfaip3* hap/del mice take on microbiota from dirty mice (P<0.001, PERMANOVA dirty mice vs SPF vs co-housed). Genotypes indicated by symbols. **(B)** Representative sections showing H&E-stained colons from female *Tnfaip3* hap/del mice 8 weeks post cohousing with dirty mice (20x magnification; scale bar = 200 µm), and **(C)** cumulative clinical score. **(D-E)** Percentage of CD44hiCD62Lo effector memory CD8+ or CD4+ T cells from the spleen (**D**) or mesenteric lymph node (**E**). **(F-G)** Percentage of CD4+FOXP3+ regulatory T cells from the spleens (**F**)

or mesenteric lymph nodes (**G**) of mice of the indicated genotypes. **(H)** FOXP3 GMFI for CD4+FOXP3+ splenic Tregs without cohousing (black bars) and post 8 weeks cohousing (red bars). FOXP3 GMFI normalised to the average GMFI of +/+ samples **(I)** Percent change in starting weights of mice with indicated genotypes given 2.5% DSS in drinking water for 5 days. Data is cumulative of two independent experiments, +/+ n=6; +/hap n=5; +/del n=8; hap/del n=8. Statistical significance determined by area under the curve analysis. **(J)** Representative haematoxylin and eosin-stained colon sections 14 days post DSS treatment and **(K)** cumulative clinical scores. **(L)** FOXP3 GMFI for CD4+FOXP3+ splenic Tregs under SPF conditions and **(M)** 14 days post DSS treatment. FOXP3 GMFI normalized to the average GMFI of +/+ samples. Statistical analysis was performed by one-way ANOVA with Tukey post hoc test unless otherwise stated, and data shown as the mean +/- s.e.m: *$P < 0.05$; ****$P < 0.0001$. ns = not significant.

668 **Methods:**
669
670 Human subjects
671 Patients and healthy family members were recruited via the Clinical Immunogenomics Research
672 Consortium Australia (CIRCA) and The Children's Hospital at Westmead, providing written informed
673 consent under protocols approved by the Sydney *Children's Hospitals* Network Human Research *Ethics*
674 Committee (SCHN HREC). Blood samples from healthy volunteers were obtained from the Australian
675 Red Cross Blood Service.
676
677 Genome sequencing
678 Parent-proband trio genomes were sequenced on the Illumina HiSeq X platform using DNA
679 isolated from whole blood, to 30x genome-wide coverage. Libraries were generated using either
680 Illumina TrueSeq PCR-free or TrueSeq Nano. Alignment, variant calling, and annotation was performed
681 as described previously (65-67).
682
683 Mice
684 To generate *Tnfaip3*^{246tr} and *Tnfaip3*^{I207L} strains, respective guide RNAs (5'- GGGATATCTGTAACACTCC
685 -3' and 5'-TGACAATGATGGGTCTTCTGAGG-3') were microinjected into C57BL/6 zygotes in
686 combination with Cas9 mRNA. For *Tnfaip3*^{I207L} strain an oligo template was also co-injected
687 (5'CTCCTCAGAGCTGAAACTCACCCAGGGAACCTAGAAACTCTCTGAGGCACCTCACCTGAAATGACAATGAG
688 GGGTCTTCTGAGAATGTTGCTGAGGACAAATATGTGGATTTCTTCCAGGGAATTGTACTGAAGTCCACTTCGG
689 GCTGCA-3'). Founder mice carrying the appropriate substitutions were then crossed to C57BL/6, and
690 heterozygous offspring intercrossed to generate homozygous, heterozygous and wild-type
691 littermates. Mice were housed at the Australian Phenomics Facility (Australian National University,
692 Canberra, Australia), or at the Australian BioResources Centre (ABR) (Moss Vale, NSW, Australia).
693 Animal studies were approved by the Garvan/St Vincent's or the Australian National University
694 Animal Ethics Committees. All procedures performed complied with the Australian Code of Practice
695 for Care and Use of Animals for Scientific Purposes.
696
697 Microbiome 16S rRNA sequencing and analysis
698 Fecal pellets from individual mice were stored at -80 prior to processing. DNA was extracted using the
699 PowerFecal DNA extraction kit (MoBio), including blanks as negative controls. 16S rRNA gene libraries
700 were prepared by amplifying the V4 region with primers that contained the 515F
701 (GTGYCAGCMGCCGCGGTAA) and 806R (GGACTACNVGGGTWTCTAAT) sequences, along with 0-3 bp
702 phasers and partial Truseq Illumina adaptors, and KAPA HiFi Hotstart ready mix for 20 amplification
703 cycles. PCR products were diluted 1:200 and amplified for a further 10 cycles with primers that
704 included the TruSeq Illumina adaptors and 6bp sample barcodes on each primer. Both DNA extraction
705 blanks and PCR negative controls were included. Final PCR products were cleaned with 0.8V JetSeq
706 Clean Beads (Bioline) and PCR yield measured with a Quant-it PicoGreen ds DNA assay
707 (ThermoFisher). Samples with a detectable PCR yield were pooled at an equimolar concentration,
708 while negative controls or samples that had no detectable yield were added to the pool at the median
709 volume used for all other samples. The pool was quantified with a Bioanalyser HS DNA chip. The
710 library was sequenced on an Illumina MiSeq using a V2 flow cell with 2 x 250 bp paired end reads.
711
712 Sequencing data was assessed for quality using FastQC, and processed using Qiime2 v 2019.10 (68). In
713 brief, primers and spacers were trimmed using cutadapt (69), forward and reverse reads were merged
714 using vsearch (70) and sequences were quality filtered and denoised to amplicon sequence variants
715 (ASVs) using Deblur (71). ASVs were classified using a naive Bayes machine-learning classifier (72)
716 trained on the V4 region of the Greengenes 16S rRNA gene operational taxonomic unit (OTU) database
717 clustered at 99% (accessed from https://docs.qiime2.org/2019.10/data-resources/ in November
718 2019). A rooted phylogenetic tree was constructed using the phylogeny plu-in and align-to-tree-

719 mafft-fasttree command. Differential relative abundance analysis was performed using the
720 composition plug-in and ANCOM (73).
721
722 Further analysis was performed in the R environment. Phyloseq (74) was used to import and transform
723 ASV counts and sample metadata. Samples with less than 10x the largest sequence count of any
724 negative controls were removed from the analysis. ASV counts were log transformed prior to
725 calculating weighted and unweighted unifrac distances using a Phyloseq wrapper of FastUnifrac (75),
726 and used as input for Principal Coordinates Analysis in Phyloseq. Significant differences in clustering
727 were assessed with PERMANOVA (76) via the adonis function of Vegan (77). Faith's phylogenetic
728 diversity (78) was calculated with Picante (79) and differences in diversity between groups assessed
729 with ANOVA in base R. Data frames were manipulated using dplyr (80) and plots generated with
730 ggplot2 (80).
731
732 Immunohistochemistry
733 Tissues were fixed in 10% neutral buffered formalin (Sigma-Aldrich), paraffin embedded and
734 sections (5 μm) prepared and stained with hematoxylin and eosin (H&E; Sigma-Aldrich). For clinical
735 scoring 4-6 random field of views at 10x magnification from three sections 500 μm apart were
736 assessed per colon. Scoring of colons from non-DSS treated mice was carried out as described by Erben
737 et al 2014 (81), Scoring scheme 2 for colonic inflammation mediated by luminal antigens. Briefly, colon
738 sections were scored (1-4) according to two criteria, a) the severity of inflammatory cell infiltrate and,
739 b) epithelial changes including hyperplasia, goblet cell and crypt loss. The scores for each criteria were
740 averaged to give the final score, with 4 representing the highest score. Scoring of colons from DSS
741 treated mice was carried out as described by Erben et al 2014 (81). Briefly, colon sections were scored
742 on four criteria, 1, Inflammatory cell infiltrate, 2, erosion and ulceration, 3, submucosal edema and
743 hyperplasia and 4, loss of crypts and goblet cells, for a total clinical score of 12. Images were captured
744 using a Leica DM 4000 or Leica DM 6000 Power Mosaic microscope (Leica Microsystems).
745
746 Flow cytometry
747 Flow cytometric staining was performed as described (15). Fluorochrome-conjugated antibody
748 clones against the following surface antigens were: CD3 (17A2), CD45.2 (104), B220 (RA3-6B2), IgD
749 (11-26), Ly6G (IA8) (Biolegend). CD4 (RM4-5), CD8 (53-6.7), CD11b (M1/70), CD23 (B3B4), CD44 (IM7),
750 FOXP3 (FJK-165) (Ebioscience). CD21 (7G6), CD25 (PC61.5), CD62L (MEL-14) CD138 (281-2), FAS (Jo2),
751 IgM (II/41) (BD Biosciences). Data were acquired with FACSCanto II and FORTESSA flow cytometers
752 (BD Biosciences) and analyzed using FlowJo software (Tree Star).
753
754 Immunoblot analysis and immunoprecipitation
755 PBMC's and murine thymocytes were lysed using lysis buffer (Cell Signaling Technology). Protein
756 concentration was measured using the Bradford assay (Bio-Rad) and total protein (20-25 μg) resolved
757 on a 7 – 10% SDS PAGE gel and then transferred to a nitrocellulose membrane, Immobilon-P® (Merck
758 Millipore). Membranes were incubated with anti-IκBα (product #: 9242), anti-A20 (Product #: 5630;
759 clone: D13H3) (Cell Signaling Technology), anti-A20 (product #: ab13597; clone: 59A426) (Abcam) or
760 anti-beta-actin (Product #: A1978; clone: AC15) (Sigma-Aldrich); followed by horseradish peroxidase
761 (HRP)-labeled secondary antibody goat-anti-mouse IgG Fc (Product #: 31433) (Pierce Antibodies) or
762 donkey-anti-rabbit IgG (Product #: NA934V) (GE Life Sciences). HRP conjugates bound to antigen were
763 detected and visualized by using an ECL detection kit (GE Life Sciences).
764
765 Real Time quantitative PCR:
766 Total RNA was extracted using the RNeasy Plus Mini Kit (Qiagen) and reverse transcribed using
767 Quantitect Reverse Transcription Kit (Qiagen). Primers were designed using Primer3 (82) with
768 sequences obtained from GenBank and synthesized by Sigma Aldrich (Supplementary Table 1). PCR
769 reactions were performed on the LightCycler® 480 Real Time PCR System (Roche) using the FastStart

770 SYBR Green Master Mix (Roche). *RPL13A* and ACTB were used as housekeeping genes and data
771 analysed using the 2ΔΔCT method. Initial denaturation was =performed at 95° C for 10 sec, followed
772 by a three-step cycle consisting of 95° C for 15 sec =(4.8° C/s, denaturation), 63° C for 30 sec (2.5°
773 C/sec, annealing), and 72° C for 30 sec (4.8° C/s, elongation). A melt-curve was performed after
774 finalization of 45 cycles at 95° C for 2 min, 40° C for 3 min and gradual increase to 95° C with 25
775 acquisitions/° C.
776
777 Statistical methods
778 Results are expressed as mean +/- standard error mean (SEM). Statistical analysis was performed
779 using the Student's *t*-test or ANOVA where indicated.

780 **Supplementary Figures and legends:**

781

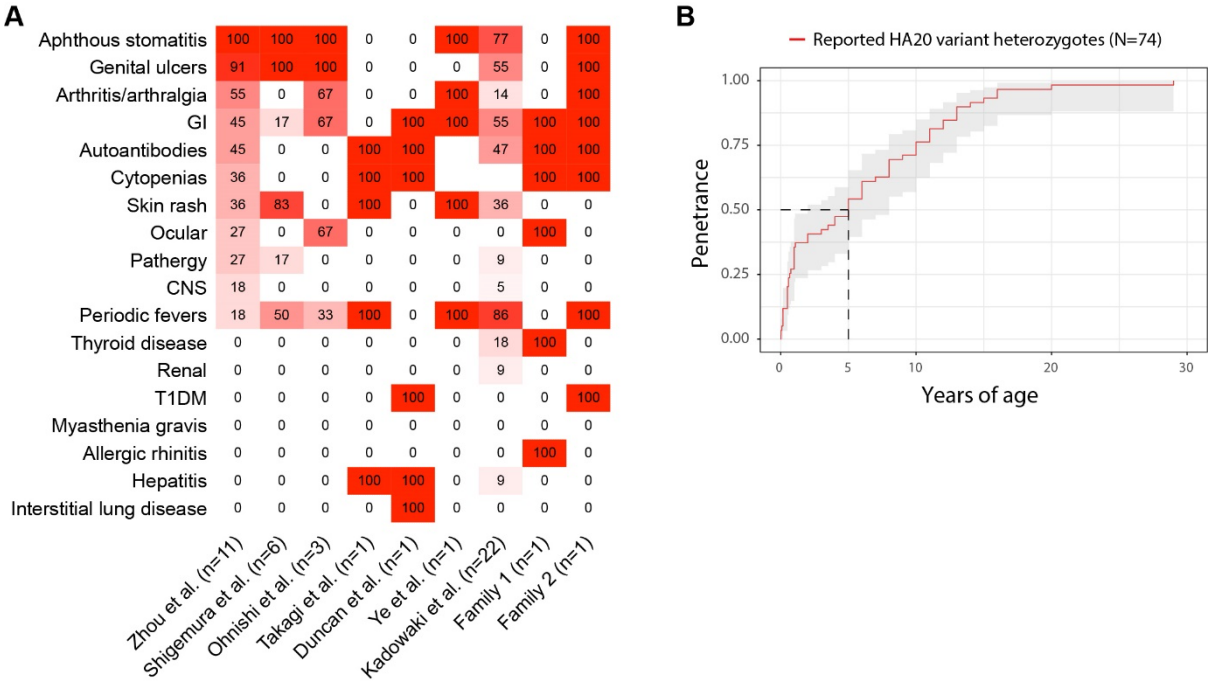

782

783 **Supplementary Figure 1**

784 **(A)** Summary of clinical presentations observed in probands from family 1 and 2 in this study,

785 compared to reported cases (18-22). **(B)** Age of disease of 74 reported HA20 variant heterozygotes.

786

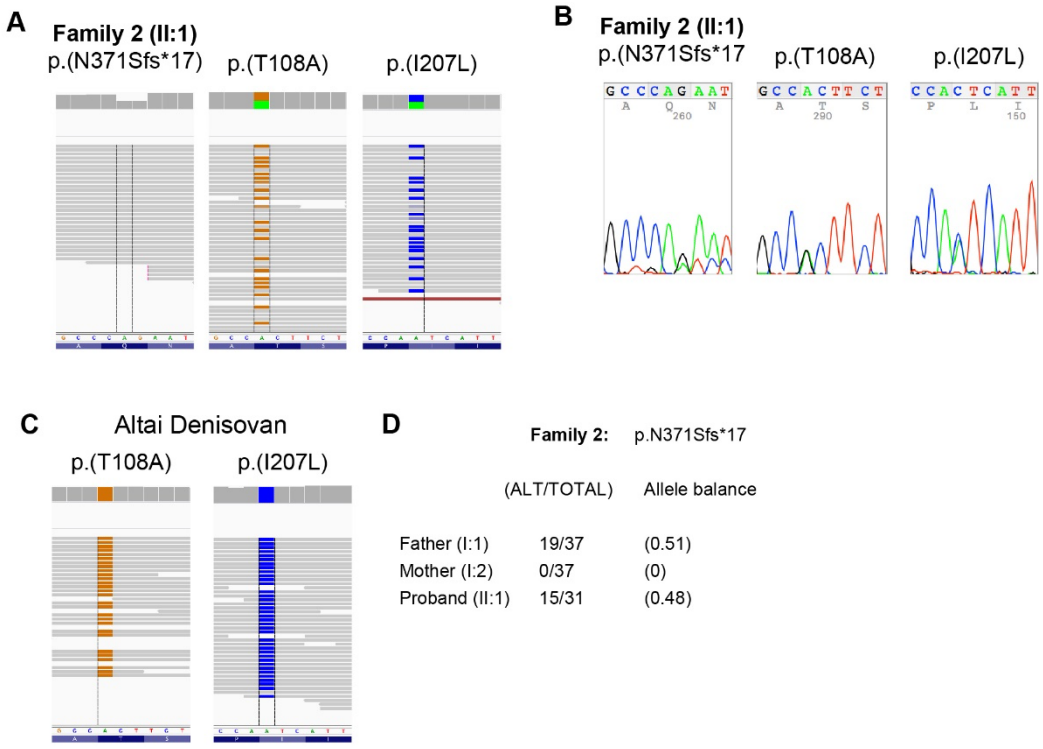

Supplementary Figure 2

(A) Read data of family 2 across TNFAIP3 frame shift (N371Sfs*17) and codols 108 and 207 **(B)** and representative chromatograms. **(C)** Read data of a high-coverage Denisovan genome (83) across TNFAIP3 codons 108 and 207. **(D)** Read call outs of p.N371Sfs*17 in family 2 trio.

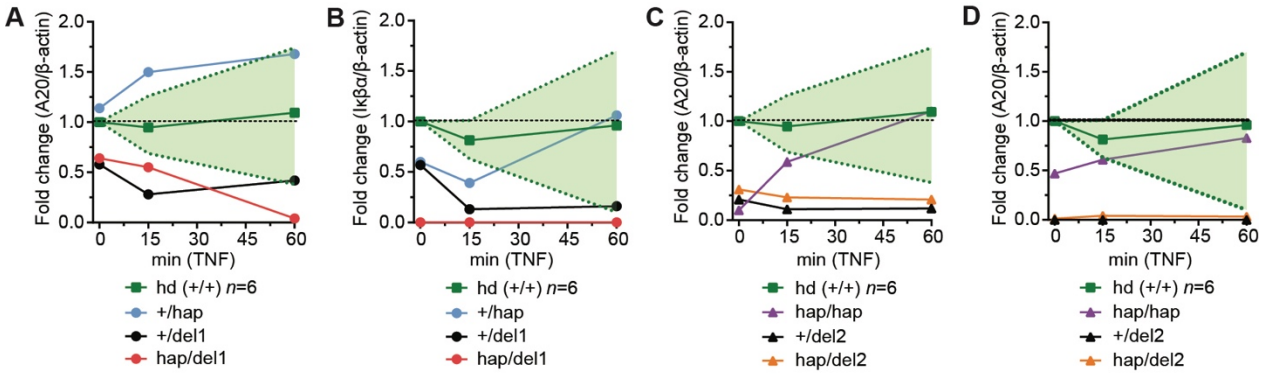

Supplementary Figure 3

(A-D) Densitometry analysis of A20 (A, C) or IκBα levels (B, D) from Trio 1 (A, B) and Trio 2 (C, D) immunoblots in Fig 2A, B. Six healthy donor (Hd) values presented as +/- range (light green shade).

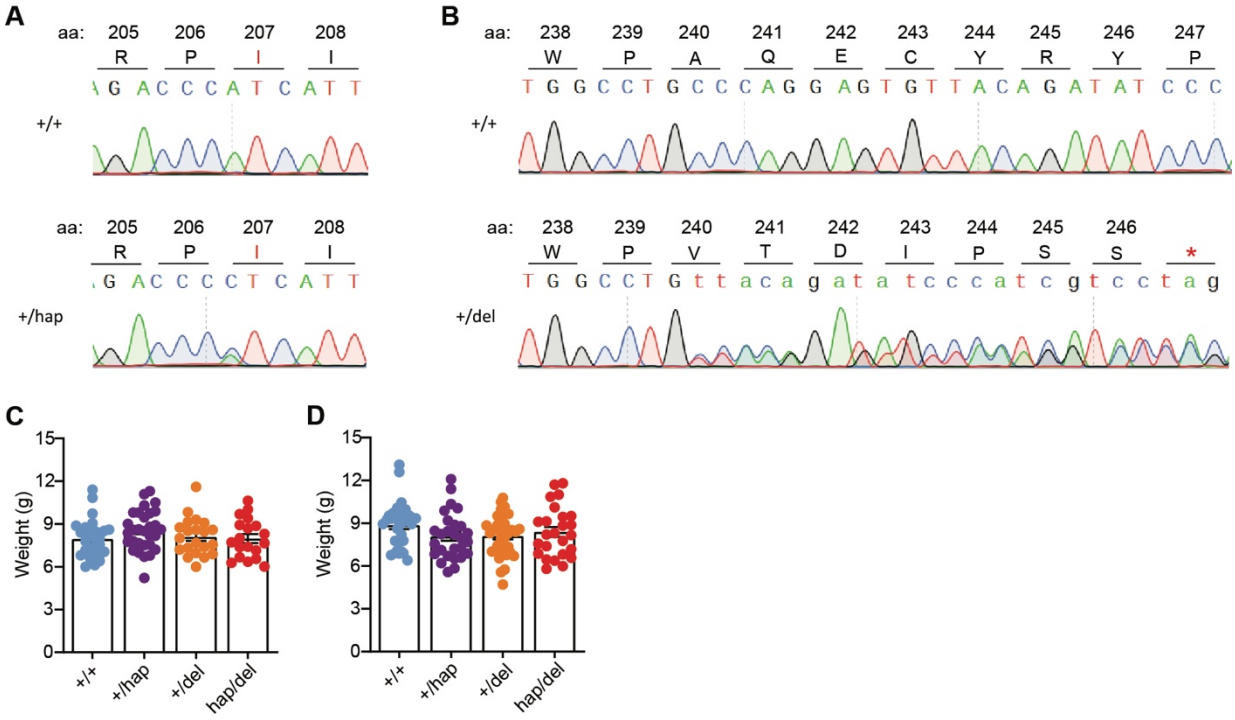

Supplementary Figure 4.
(A) Representative Sanger chromatogram for mice with the I207L (hap) or **(B)** A240Vfs*7 (del) alleles. **(C-D)** Weight of 8-week-old female (C) or male (D) *Tnfaip3* hap/del mice of the indicated genotype.

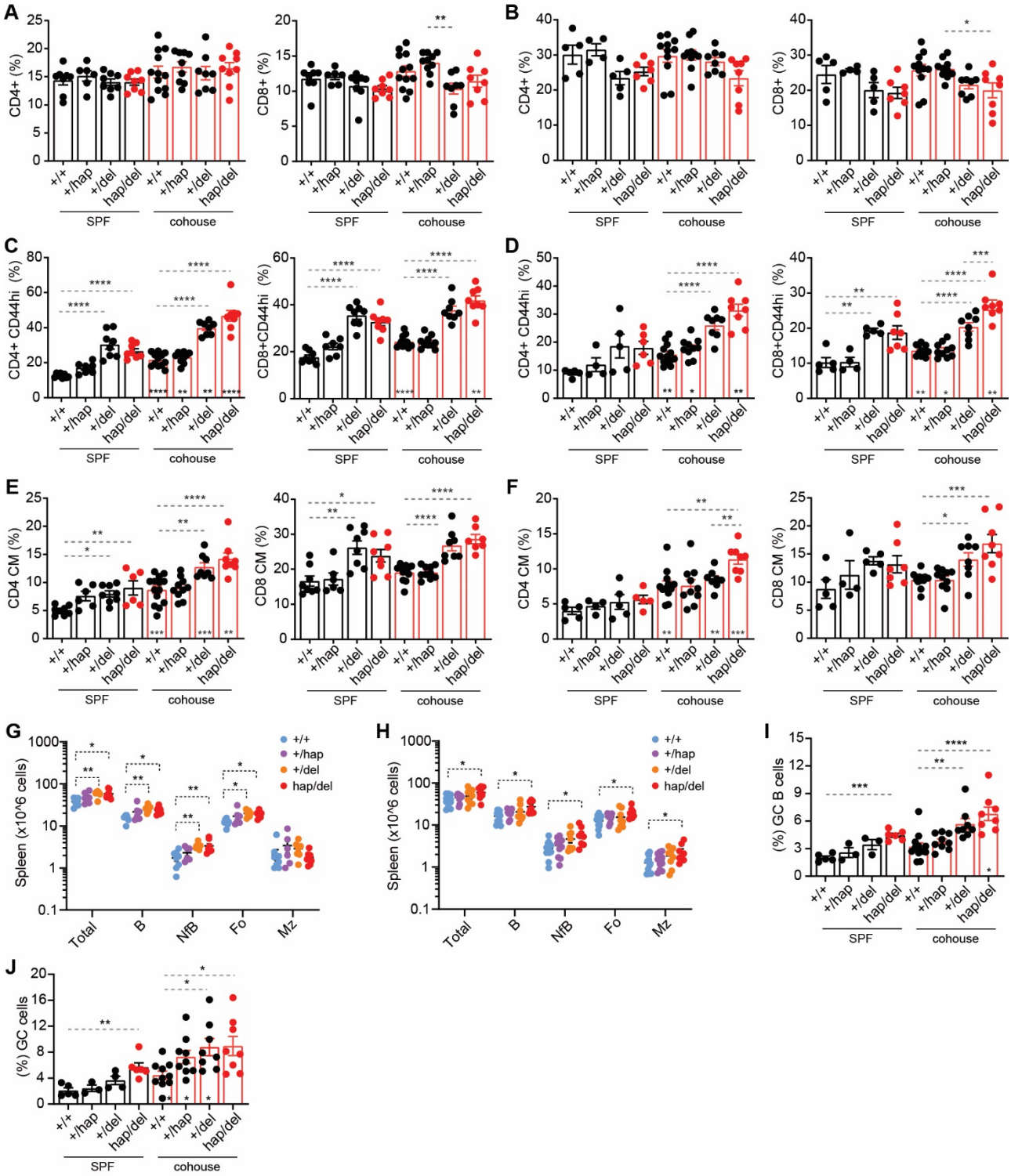

Supplementary Figure 5.

(A-F) Flow cytometry analysis of splenic (A, C, E) or mesenteric lymph node (B, D, F) T cell populations from Tnfaip3I207L/246tr mice housed under SPF conditions (black bars) or cohoused with dirty mice for 8 weeks (red bars). **(A, B)** Percentage of CD4+ or CD8+ T lymphocytes. **(C, D)** Percentage of CD4+ or CD8+ CD44hi memory T cells. **(E, F)** CD44hiCD62hi central memory CD8+ or CD4+ T cells. **(G, H)** Absolut numbers of B cells in the spleen of individual mice with the indicated *Tnfaip3* genotype, in SPF conditions (G) or post cohouse with dirty mice for 8 weeks (H). B, B cells; NFB, newly formed B cells; FO, follicular B cells; MZ, marginal zone B cells.

811 **(I-J)** Flow cytometry analysis of splenic (I) or mesenteric lymph node (J) B cell germinal centres. **(K-M)**
812 Percent proportions of splenic inflammatory monocytes (K), neutrophils (L) and NK1.1 (M) positive
813 cells were also assessed.**n**Statistical analysis was performed by one-way anova ANOVA with Tukey
814 post hoc test, and data shown as the mean +/- s.e.m: *$P < 0.05$; **$P < 0.01$; ***$P < 0.001$; ****$P <$
815 0.0001. ns = not significant.

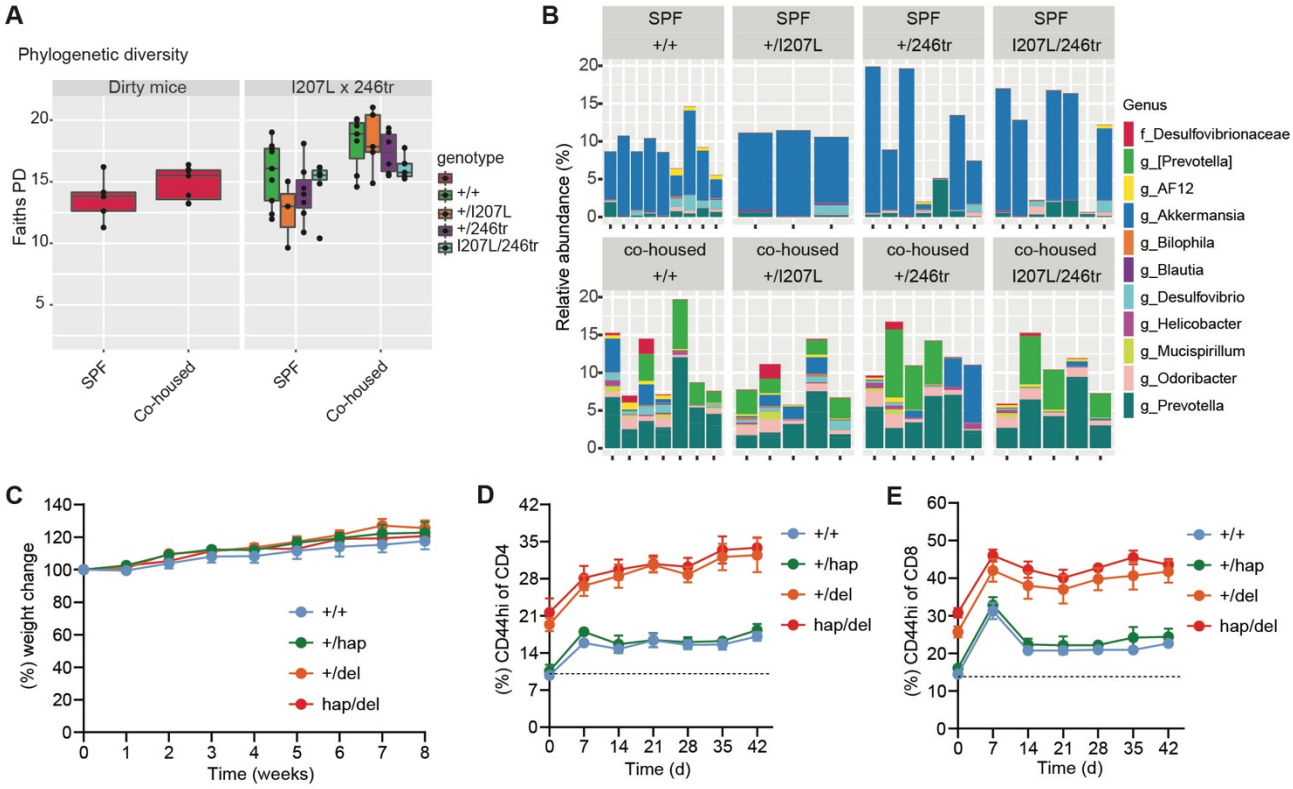

Supplementary Figure 6.

(A) Bar plot showing relative abundance of significantly changing bacteria species following cohousing ($p<0.05$, two-way ANOVA). **(B)** Weekly weights presented as percent change in starting weight, for *Tnfaip3* hap/del mice of the indicated genotypes cohoused with dirty mice (+/+ n=4; +/hap n=5; +/del n=3; hap/del n=3). **(C)** Percent CD44hi CD8+ T cells or **(D)** CD44hi CD4+ T cells in the blood of *Tnfaip3* hap/del mice co-housed with dirty mice (+/+ n=7; +/hap n=6; +/del n=5; hap/del n=5).

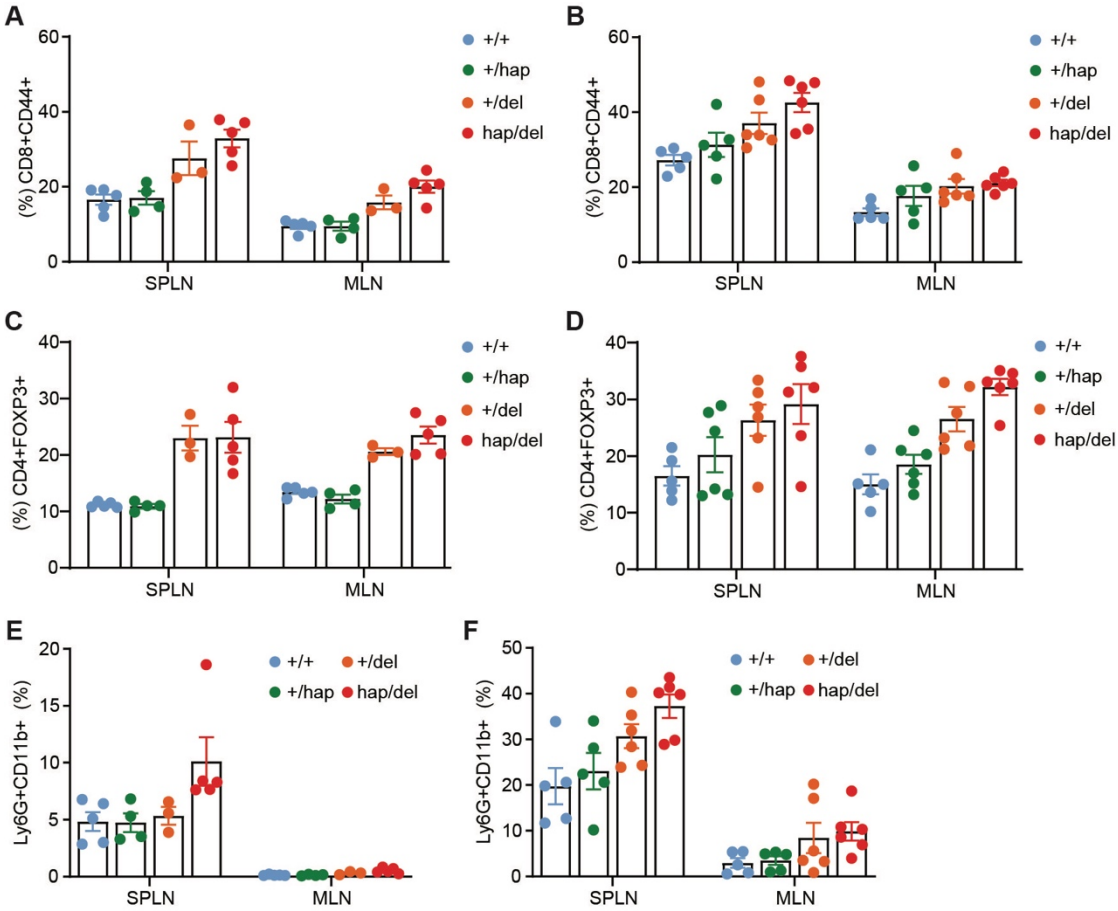

Supplementary Figure 7.

(A, B) Percentage of CD44hi CD8+ or CD4+ T cells from the spleen (SPLN) or Mesenteric lymph node (MLN) of *Tnfaip3* hap/del mice of the indicated genotype (B) before or (C) 14 days post DSS treatment. **(C, D)** Percentage of CD4+FOXP3+ cells from the spleen (SPLN) or Mesenteric lymph node (MLN) of *Tnfaip3* hap/del mice of the indicated genotype (D) before or (E) 14 days post DSS treatment. **(E, F)** Percentage of CD45+Ly6G+CD11b+ neutrophils from the spleen (SPLN) or Mesenteric lymph node (MLN) of *Tnfaip3* hap/del mice of the indicated genotype (F) before or (G) 14 days post DSS treatment.

831 **Supplementary Tables**

832 **Supplementary Table 1.**

833 Human primers used for qRT-PCR analysis.

Gene	Primer sequence
ACTB	F- 5'-CATCGAGCACGGCATCGTCA-3' R- 5'-TAGCACAGCCTGGATAGCAAC-3'.
CXCL2	F- 5'-AGGGAATTCACCTCAAGAACATCC-3' R- 5'-TGTGGCTATGACTTCGGTTTGG-3'
ICAM1	F- 5'-AGTTGCTCCTGCCTGGGAAC-3' R- 5'-TTTAGCTGTTGACTGCCCATCAG-3'
RPL13A	F- 5'-CAAGCGGATGAACACCAAC-3' R- 5'-TGTGGGGCAGCATACCTC-3'
TNFAIP3	F- 5'-AACGAACGGTGACGGCAAT-3' R- 5'-GAAGTCCACTTCGGGCCAT-3'
TNF	F- 5'-TCCCCTGGAAAGGACACCAT-3' R- 5'GGGTTTGCTACAACATGGGCT-3'

834